Proceedings of ISFOG 2025
5TH INTERNATIONAL SYMPOSIUM ON
FRONTIERS IN OFFSHORE GEOTECHNICS
Nantes, France | June 9-13 2025

ISBN 978-2-85782-758-0

Evaluating Soil Reaction Models for Offshore Wind Turbine Monopile Foundations: Implications for ULS and FLS Design

J. Tott-Buswell*
University of Nottingham, Nottingham, United Kingdom

S. Delgado-Trujillo, L. J. Prendergast
University of Nottingham, Nottingham, United Kingdom

S. Jalbi, J. Hilton, S. Berberic

Sea and Land Project Engineering, London, United Kingdom

jacques.tott-buswell1@nottingham.ac.uk (corresponding author)

ABSTRACT: To meet crucial Net Zero goals, increasingly large Offshore Wind Turbines (OWTs) are being deployed in deeper waters. This trend has heightened the dynamic sensitivity to environmental loads, making monopile foundations vulnerable to large strain cycles. Time domain simulations using linearised beam-spring models are commonly employed to facilitate ULS and FLS analysis under representative wind and wave loads during an OWT's operational life. However, the dynamic response of OWT-monopile systems is dependent on the unloading behaviour of the spring elements. This paper examines the effects of three distinct soil reaction models on the dynamic response of a monopile. These are: i) Linear, ii) Nonlinear elastic, and iii) Hysteretic. For FLS analysis, a random wave load model is employed, and the damage after 25 years is estimated using the Damage Equivalent Moment (DEM). For ULS, extreme wave events are simulated by imposing a constrained wave onto a random wave and calculating the location and value of the maximum moment along the monopile. Results suggest that the hysteresis model reduces the expected damage after 25 years due to material damping, and nonlinear spring models in general experience larger maximum bending moments at lower depths. The hysteresis model is shown to retain the plastic strains due to the extreme event.

Keywords: Soil-Structure Interaction; Offshore Wind Turbines; Monopile Foundation Design;

1 INTRODUCTION

The Offshore wind sector is rapidly expanding to meet rising renewable energy demands (Wind Europe, 2021). Fixed-bottom OWTs, predominantly supported by monopiles due to the relative ease of fabrication and installation, are facing increasingly demanding loading conditions. Monopile systems are design within the "soft-stiff" frequency range, avoiding resonance with rotor and external loads (1P and 3P blade passing frequencies). However, as rotor sizes grow and the rotations per minute decrease, this range narrows, potentially overlapping with lower wave-induced excitation frequencies. This overlap increases strain amplitudes in soil and structural elements, impacting system longevity.

The dynamic sensitivity of large OWT-monopile systems demands robust modelling to satisfy Ultimate, Fatigue, and Serviceability Limit States (ULS, FLS, SLS). Frequency-domain methods facilitate analyses of environmental force frequencies efficiently (Dirlik, 1985), but fail to account for nonlinearity without complex modifications (Alexander, 2010; Huang *et al.*, 2018). Nonlinear soil behaviour is better addressed through time-domain finite element analyses, where equilibrium is solved iteratively. However, these methods must appropriately replicate the plasticity and unload-reload behaviour of the soil during large strains, which can be computationally demanding. While frequency-domain analysis is faster, it neglects hysteretic soil damping, which is critical for dynamic behaviour and capable of dissipating up to 5% of the first mode's energy (Tarp-Johansen *et al.*, 2009).

The design process involves evaluating numerous sea states, highlighting the need for computational efficiency. Balancing computational cost and accuracy in modelling soil-structure interaction for dynamic analyses remains a challenge. This paper examines the impact of soil unload-reload behaviour in dynamic simulations of a 15 MW OWT supported by a monopile. A representative ULS and FLS design process is assessed across three distinct soil unloading

mechanisms, with the resulting design implications analysed.

2 METHODOLOGY

A one-dimensional OWT-monopile model that integrates structural dynamics, nonlinear soil-structure interaction, and environmental loads is developed for this analysis. The finite element model uses Timoshenko beam elements (Friedman and Kosmatka, 1993), with lateral support from horizontal springs at nodes below the mudline, following a Winkler beam-spring approach (Figure 1(a)). The environmental loads are modelled by temporally fixing a wind force at the Rotor-Nacelle Assembly (RNA) position as a point load, and wave forces as spatially and temporally varying distributed loads below the generated wave elevation η. Structural damping is considered using Rayleigh's viscous damping method where the first and second modes of fore-aft vibration are targeted. It is noted that aerodynamic damping is not considered in this analysis, therefore this configuration is representative of idling conditions.

Two wave models are considered: a constrained wave, which is typically used to model extreme events appropriate for ULS analyses, and linear random wave theory, which models irregular sea states used in FLS analyses. The wind load is modelled as an equivalent static thrust force at the top node, as is common in engineering assessments. The influence of the unloading spring behaviour on design outcomes is assessed by examining three spring models mechanisms for both ULS and FLS. The details of the wave and soil-structure interaction models are presented in the following sections.

2.1 Soil models

The soil-structure interaction is often represented through empirically derived nonlinear *p-y* relationships, where '*p*' denotes lateral resistance and '*y*' denotes local pile deflection (Reese, Cox and Koop, 1974; Jeanjean *et al.*, 2011). However, the unloading behaviour of the *p-y* relationship needs to be defined for time-domain simulations. The *p-y* curve is used to describe the behaviour of the three spring models investigated.

Figure 1(b) shows the simple linear spring model, where *p* can be calculated as:

$$p = ky \tag{1}$$

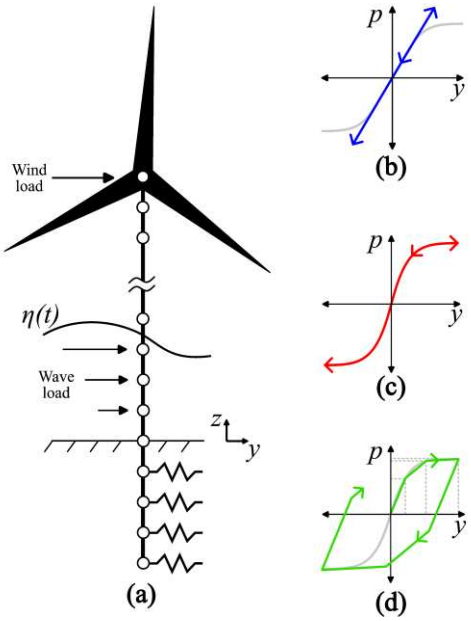

Figure 1. (a) A schematic of the beam-spring finite element model with SSI and the force-displacement curves of the soil models; (b) linear, (c) nonlinear elastic and (d) piece-wise hysteresis

where k is the initial tangent stiffness of the *p-y* function. This gives a poor representation of lateral reaction forces at large strains. Alternatively, the original *p-y* curve can be traced such that the restoring force reaches a maximum at large strains and returns along the same stress path when unloaded (Figure 1(c)). It follows that,

$$p = f(y) \tag{2}$$

where $f(y)$ is the nonlinear *p-y* function. This approach offers the simplest implementation of soil nonlinearity in dynamic analysis. It is well-established that laterally loaded piles do not return along the same stress paths when unloaded. Instead, a plastic deformation is retained after unloading, with a deformation path reflecting the initial stiffness k (McAdam *et al.*, 2020). This also becomes a source of energy dissipation and can be modelled using a kinematic hardening approach. The third spring model therefore employs an Iwan model to encapsulate Masing-type hysteresis behaviour, as shown in Figure 1(d) (Iwan, 1967). The *p-y* curve is discretised into N elements such that:

$$p = \sum_{i=1}^{N} k_i (y_s - y_{p,i}) \tag{3}$$

where y_s is the total displacement of the node. k_i and $y_{p,i}$ denotes the initial stiffness and plastic deformation of the i^{th} elastic-perfectly plastic spring element,

respectively, and is informed from a piecewise *p-y* curve of *N* linear segments. Figure 2 demonstrates the unloading behaviour of the i^{th} bilinear spring element.

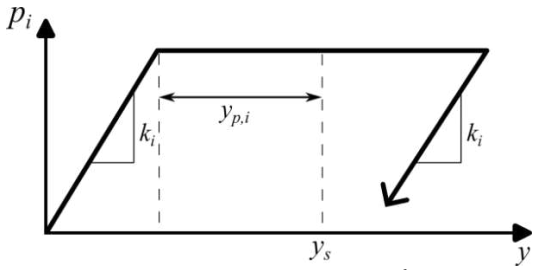

Figure 2. Unloading behaviour of the i^{th} bilinear spring element

The sum of *N* elements loaded in parallel therefore produces a globally hysteretic response as shown in Figure 1(d) which will inherently capture large-strain soil damping effects (Beuckelaers, 2017).

2.2 Wave loading

Wave loads are calculated by determining a free surface elevation $\eta(t)$ at the location of the monopile and the kinematics along the substructure are calculated using Airy's theory. Morison's equations determine drag and inertial forces based on the velocity and acceleration profile, respectively. Wheeler's stretching is applied to vertically adjust the calculated wave kinematics to the free surface elevation profile.

For FLS analysis, a random surface elevation is derived by decomposing the Power Spectral Density (PSD) of a sea state, which depends on the significant wave height (H_s) and the peak wave period (T_p). The JONSWAP spectrum is used in this study.

For ULS analysis, the largest wave height H_{max} is combined with randomly generated wave elevations using PSD decomposition to form a constrained wave. Both wave models are illustrated in Figure 3.

2.3 Wind loading

A fixed wind load is used to model the aerodynamic force by applying a constant load at the top node, which is a common method in early design stages. This ensures a one-way cyclic response in the ground model.

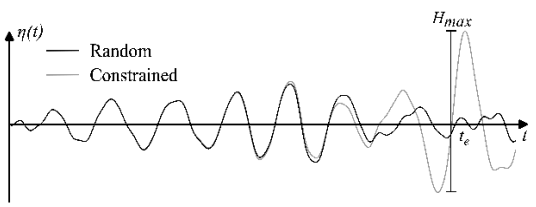

Figure 3. Sea surface elevation at the monopile's location for random and constrained waves

3 CASE STUDY

A 15 MW OWT-monopile system is informed using design-based mass distributions and geometric parameters, incorporating generalised masses and sectional properties as lumped masses and beam elements, respectively. Key geometry features are described in Table 1 and 2.

Table 1. Tower properties

Parameter	Value
Length	125 m
Diameter (lower-upper)	8 m – 6.50 m
Wall thickness (min.-max.)	0.020 m – 0.075 m
RNA mass	815,000 kg

Table 2. Monopile properties

Parameter	Value
Full length	110 m
Embedded length	27.5 m
Cone length	24 m
Diameter (lower-upper)	11.5 m – 8 m
Wall thickness	0.08 m

The *p-y* curves in this study are derived from discrete lateral reaction forces obtained through three-dimensional pile-soil finite element analyses (Whyte *et al.*, 2020).

For extreme events, the parameters of the constrained wave model are selected to be representative of a 50-year return period. Sixty waves are simulated, and the maximum bending moment profiles are reviewed for each soil reaction model.

For fatigue events, two sea states are derived from different H_s-T_p scatter tables. These scatter tables contain the probability of occurrence of a given sea state over a 25-year period, as shown in Figure 4. Figure 4(b) shows a high probability of occurrence around the natural period of the system, which was calculated to be T_n = 6.8 seconds using an eigenvalue analysis. The effects of dynamic amplification in FLS analyses are therefore also investigated. The Damage Equivalent Moment (DEM) at the mudline is determined for each soil reaction model by cycle-counting the bending moments and applying a Palmgren-Miner rule. The DEM is used as a metric to quantify the anticipated damage after 25 years and refers to the moment amplitude that would produce the same damage after 10^7 uniform cycles. Relevant wave parameters for the ULS and FLS design case are provided in Table 3. The wind load for the ULS and FLS case study have been identified externally and applied to the model.

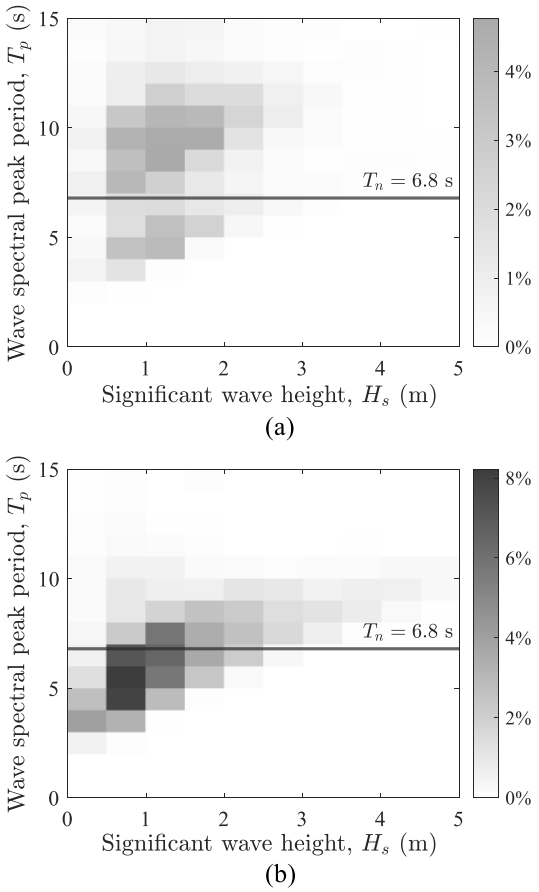

Figure 4. Probability of occurrence of sea states over 25 years for (a) sea state A and (b) sea state B.

Table 3. Wave properties

Parameter	ULS (constr.)	FLS (random)
Mean sea water level, d	60.0 m	60.0 m
Significant wave height, H_s	8.0 m	0.25 – 8.25 m
Peak period, T_p	12.0 m	0.5 – 24.5 m
Maximum height, H_{max}	16.0 m	-
Wave occurrence, t_e	500 s	-

Time-domain simulations are performed using the Constant Average Acceleration Newmark-β time integration scheme with Newton-Raphson iterations to achieve equilibrium. Simulations are run for 800 seconds at 0.05-second time steps and the code is developed in MATLAB. The first 200 seconds of the response are ignored to avoid the initial transient response in the analysis. N = 45 bilinear springs are used to define the hysteresis reaction model in Equation (3). A Rayleigh damping ratio of 1% is applied to the first and second fore-aft vibration modes for all simulations.

4 RESULTS

4.1 FLS design

A range of sea states are generated from the scatter table shown in Figure 4(a) and 4(b), and the DEM is calculated along the monopile for each soil model described in Equations (1) to (3). The maximum DEM along the monopile is recorded. The results are presented in Table 4 as a percentage difference compared to the linear model.

Table 4. DEM percentage difference of soil models against linear model

Sea state	Soil reaction model	DEM % diff.
A	Nonlinear elastic	+1.47%
	Hysteresis	-0.58%
B	Nonlinear elastic	+2.59%
	Hysteresis	-1.11%

Both sea states suggest that the nonlinear elastic model produces the highest DEMs. This is due to the soft unloading behaviour when mobilised by large strain cycles, leading to larger deflections compared to the linear model. Conversely, the hysteresis model retains the original stiffness of the system when unloaded, reducing the amplitude of the strain cycles and therefore the damage in the structural members. Additionally, the hysteretic damping will lower the deflections and therefore the DEM.

The percentage difference is larger in sea state B is larger than sea state A due to the structure resonating with the wave loads. The nonlinear model exhibits more damage due to the dynamic amplification, whereas the hysteresis model demonstrates less damage. The hysteresis model is therefore better suited for FLS analyses, especially when dynamic amplifications are expected.

It should be noted that it is difficult to discern the contribution of dynamic amplification from the linear model, which is likely to occur in these simulations due to the low viscous damping. This may contribute to a larger DEM in the linear model. Additionally, it is common design practice to linearise *p-y* curves at a representative load level. This was not done in this study for simplicity.

4.2 ULS design

Sixty constrained waves, with properties listed in Table 3, are generated and applied to the three soil models described by Equations (1) through (3). For each simulation, the maximum moment at the mudline and the global maximum moment are recorded and normalised to the maximum moment in the linear

model (M_L). The maximum moments are plotted in Figure 5 and the average depth at which they occur are recorded in Table 5.

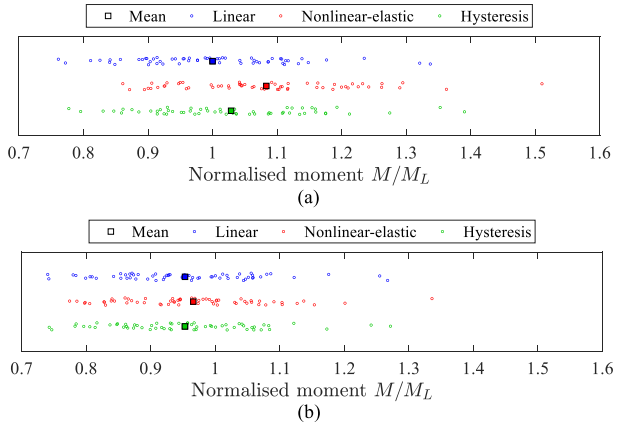

Figure 5. (a) Maximum global bending moments and (b) maximum moment at the mudline

Table 5. Average depth of maximum global moment for each soil reaction model

Soil model	**Average depth (z)**
Linear	-4.35 m
Nonlinear elastic	-7.91 m
Hysteresis	-6.24 m

The spread of data in Figure 5 is indicative of the dynamic sensitivity of the OWT-monopile system to irregular sea state prior to the extreme event. Direct comparison of bending moment profiles between different simulations is therefore not possible, as the kinematics of the tower (and hence the deflections of the monopile) may be out of phase when the maximum moments occur.

Figure 5(a) and Table 5 show that the global maximum moment varies in both magnitude and location depending on the spring model used. The nonlinear-elastic model demonstrated the largest moment at the greatest depth. During the extreme event, large strains in the nonlinear-elastic and hysteresis models mobilise the weaker springs near the surface, reducing their stiffness. This stiffness variation along the embedment shifts the maximum moment location downward. Nonlinear soil-structure interaction will therefore influence the cross-sectional properties of monopile segments, as an appropriate wall thickness would need to be selected to ensure compliance with the ULS design utilisations.

The maximum moment at the mudline that occurs during constrained wave simulations is often used to iteratively design the required penetration depth and diameter of the monopile. Figure 5(b) suggests that the type of unloading behaviour would have a negligible influence on this process. The observed bending moment trends may be specific to the tested soil profile, highlighting the need for further site investigations.

Figure 6 presents the mudline deflection time history for each soil reaction model. The average displacement remains above zero due to the fixed wind load. The nonlinear-elastic and hysteresis models exhibit higher average displacement due to plastic deformation. Notably, the hysteresis model retains plastic deformation after the large wave, effectively capturing the large-strain soil response.

5 CONCLUSIONS

This paper evaluates three soil-structure interaction models for the dynamic analysis of an OWT monopile system using site-specific *p-y* reaction curves with distinct unloading behaviours. Performance is assessed in ULS and FLS contexts by simulating constrained and random waves, respectively. A fixed wind load is applied at the RNA position to encourage one-way response. A consistent 1% damping ratio is applied to simulate idling conditions and minimal aerodynamic damping. The performance of the nonlinear-elastic and hysteresis spring models is assessed relative to the linear spring model. The hysteresis model demonstrated an improved fatigue performance by producing less damage in the structural members, especially under resonant conditions. The hysteresis model may offer improved cost-effectiveness in monopile sizing due to the reduced damage. The ULS analysis demonstrated that

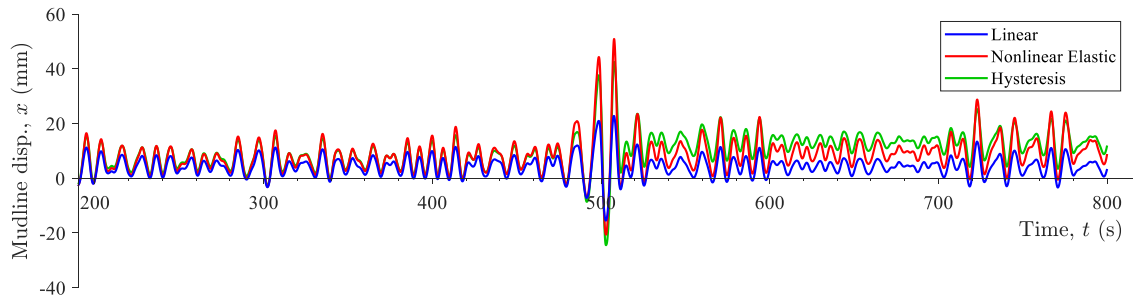

Figure 6. Time history of mudline deflections for each soil reaction model during a constrained wave simulation

the nonlinear-elastic model produced the largest maximum global bending moment on average which would lead to conservative design outputs, and the hysteresis model retained plastic deformations after the large wave impact. The mudline moments were generally unaffected by spring type; however, the location of the maximum moment was deeper for the nonlinear models. This will influence the sectional properties of the monopile.

These findings are based on a specific design case and may vary with site-specific ground and environmental conditions. Further studies, including laboratory validation, are needed to generalise the results. Wind turbulence effects, which could impact DEM results by adding cyclic loads and increasing aeroelastic damping, were not considered.

AUTHOR CONTRIBUTION STATEMENT

J. Tott-Buswell: Data Curation, Formal Analysis, Investigation, Methodology, Software, Validation, Visualisation, Writing – Original Draft. **S. Delgado-Trujillo:** Methodology, Software, Visualisation, Writing – Original Draft, Writing – Review and Editing. **L. J. Prendergast:** Funding Acquisition, Project Administration, Supervision, Writing – Review and Editing. **S. Jalbi:** Conceptualisation, Project Administration, Supervision, Writing – Review and Editing. **J. Hilton:** Conceptualisation, Project Administration, Supervision, Writing – Review and Editing. **S. Berberic:** Supervision, Software, Writing – Review and Editing.

ACKNOWLEDGEMENTS

The authors are grateful for the financial support provided by UKRI through Innovate UK and the KTP initiative. FRONTIErS DN has received funding from the European Union's Horizon Europe Programme under the Marie Skłodowska–Curie actions HORIZON-MSCA-2021-DN-01 call (Grant agreement ID: 101072360), and from UK Research and Innovation (Grant Ref: EP/X027910/1 and EP/X027821/1)

REFERENCES

Alexander, N. (2010) 'Estimating the nonlinear resonant frequency of a single pile in nonlinear soil', *Journal of Sound and Vibration*, 329(8), pp. 1137–1153. Available at: https://doi.org/10.1016/j.jsv.2009.10.026.

Beuckelaers, W. (2017) *Numerical modelling of laterally loaded piles for offshore wind turbines*. Oxford University.

Dirlik, T. (1985) *Application of computers in fatigue analysis*. University of Warwick.

Friedman, Z. and Kosmatka, J.B. (1993) 'An improved two-node timoshenko beam finite element', *Computers & Structures*, 47(3), pp. 473–481. Available at: https://doi.org/10.1016/0045-7949(93)90243-7.

Huang, X.-R. *et al.* (2018) 'Nonlinear modal synthesis for analyzing structures with a frictional interface using a generalized Masing model', *Journal of Sound and Vibration*, 434, pp. 166–191. Available at: https://doi.org/10.1016/j.jsv.2018.07.027.

Iwan, W.D. (1967) 'On a Class of Models for the Yielding Behavior of Continuous and Composite Systems', *Journal of Applied Mechanics*, 34(3), pp. 612–617. Available at: https://doi.org/10.1115/1.3607751.

Jeanjean, P. *et al.* (2011) *A Framework for monotonic p-y curves in clays*, *Proceedings of the 20th USENIX Security Symposium*.

McAdam, R.A. *et al.* (2020) 'Monotonic laterally loaded pile testing in a dense marine sand at Dunkirk', *Géotechnique*, 70(11), pp. 986–998. Available at: https://doi.org/10.1680/jgeot.18.PISA.004.

Reese, L.C., Cox, W.R. and Koop, F.D. (1974) 'Analysis of Laterally Loaded Piles in Sand', in *All Days*. Reston, Virginia: OTC, pp. 95–105. Available at: https://doi.org/10.4043/2080-MS.

Tarp-Johansen, N.J. *et al.* (2009) 'Comparing Sources of Damping of Cross-Wind Motion', *Proceedings of European Offshore Wind 2009 : Conference & Exhibition*, pp. 1–10.

Whyte, S.A. *et al.* (2020) 'Formulation and implementation of a practical multi-surface soil plasticity model', *Computers and Geotechnics*, 117, p. 103092. Available at: https://doi.org/10.1016/j.compgeo.2019.05.007.

Wind Europe (2021) *Wind Energy in Europe: 2021 Statistics and the outlook for 2022-2026*.